
Nabil Simaan*
Moshe Shoham

Robotics Laboratory
Department of Mechanical Engineering
Technion-Israel Institute of Technology
Haifa 32000 ISRAEL
nsimaan@cs.jhu.edu
shoham@tx.technion.ac.il

Stiffness Synthesis of a Variable Geometry Six-Degrees-of-Freedom Double Planar Parallel Robot

Abstract

In this paper, we address the stiffness synthesis problem of variable geometry double planar parallel robots. For a desired stiffness matrix, the free geometrical variables are calculated as a solution of a corresponding polynomial system. Since in practice the set of free geometrical variables might be deficient, the suggested solution addresses also the case where not all stiffness matrix elements are attainable. This is done through the use of Gröbner bases that determine the solvability of the stiffness synthesis polynomial systems and by transforming these systems into corresponding eigenvalue problems using multiplication tables. This method is demonstrated on a novel variable geometry double planar six-degrees-of-freedom robot having six free geometric variables. A solution of the double planar stiffness synthesis problem is obtained through decomposing its stiffness matrix in terms of the stiffness matrices of its planar units. An example of this procedure is presented in which synthesizing six elements of the robot's stiffness matrix is obtained symbolically and validated numerically yielding 384 real solutions.

KEY WORDS—parallel robot, double planar robot, reconfigurable, stiffness synthesis, Gröbner bases

1. Introduction

Robots are designed to perform various tasks that involve complex manipulations and interactions with their environment. Consequently, the performance of fixed geometry (non-redundant) robots is compromised for some tasks, e.g., a fixed geometry robot performing a task involving contact with the environment has stiffness characteristics determined by its inverse kinematics solution rather than by the task specifications. In contrast to *fixed geometry parallel robots*, using rigid

fixed geometry platforms, *variable geometry parallel robots* can change the geometry of their base/moving platforms. In the present study we focus on variable geometry robots that can change their geometry to accommodate task-based requirements of stiffness and we present a solution for double planar (DP) variable geometry robots.¹

Various methods of adding redundancy were suggested in the literature to enhance robot performances. Actuation redundancy (antagonistic actuation) was used in stiffness modulation of parallel manipulators and synthesis of RCC (Remote Center of Compliance) devices to control their stiffness and compliance center (Yi, Freeman, and Tesar 1989; Yi and Freeman 1992; Kim, Lee, and Yi 1997; Kock and Schumacher 1998). However, for robots with actuators having high stiffness values or non-back-drivable actuators, the contribution of the antagonistic actuation to the overall stiffness is diminished unless large antagonistic forces are used (Yi and Freeman 1993). Furthermore, stiffness modulation is affected by higher-order singularities (Yi and Freeman 1993; Simaan and Shoham 2003).

Kinematic redundancy of robots was used by Merlet, Preng, and Daney (2000) to design a six-degrees-of-freedom (6-DoF) Stewart–Gough robot as a five-axis milling machine. The robot's one extra DoF was used to include a desired trajectory inside the workspace of the robot and to ensure that the robot path is singularity-free. Investigations focusing on stiffness/compliance characteristics include the works of Patterson and Lipkin (1990, 1993) who classified robot compliance matrices based on their eigenscrews and twist compliant axes and discussed the relations among twist compliant axes and wrench compliant axes. Loncaric (1985) and Huang and Schimmels (1998a) characterized the space of realizable stiffness matrices using only simple springs. Other works focused on stiffness synthesis of systems of springs. Huang and Schimmels (1998b) and Roberts (1999) determined the

1. The method was also applied for special cases of Stewart–Gough robots and is a subject of a future publication.

*Mr. Simaan is currently affiliated with CISST at Johns-Hopkins University.
The International Journal of Robotics Research
Vol. 22, No. 9, September 2003, pp. 757-775,
©2003 Sage Publications

minimal number of simple springs for realizing a stiffness matrix while Ciblak and Lipkin (1999) discussed the limits on the minimal number of linear and torsional springs for achieving a general rank- r stiffness matrix. Huang and Schimmels (1998a, 1998b), Roberts (1999), and Ciblak and Lipkin (1999) presented synthesis algorithms using Cholesky decomposition of the desired stiffness matrix to compute the required springs for obtaining a desired stiffness of a system of two rigid bodies connected by springs. These algorithms considered the general synthesis problem and assumed no limitation on the geometry of the springs (connection points and spring constants).

The present investigation differs from the above-mentioned works. It suggests a method to synthesize a required stiffness with given actuator stiffness. Moreover, since in practice only a limited number of variable geometry parameters are available, the present investigation offers a scheme to determine which set of stiffness matrix elements can be synthesized.

One promising method to overcome the robot-to-task fitness problem is the use of variable geometry parallel robots. However, currently there are only a small number of works that address this approach. Among these works are the work of Zhiming and Song (1998), who investigated the design aspects of modular Stewart–Gough platforms with workspace and joint limits considerations, and the work of Zhiming and Zhenqun (1999) who presented an algorithm for identifying the parameters of the joint locations on the base in a modular Stewart–Gough platform. The recent work of Du Plessis and Snyman (2002) presented an algorithm for changing the geometry of a planar 3-DoF manufacturing robot. Their algorithm is based on minimizing an objective function defined by the overall maximal magnitude of the actuator forces for a given desired path. These forces were updated by the inverse dynamics model of the robot. The optimization was constrained with given limits on the length of the actuators.

Recently, Simaan and Shoham (2002) investigated a variable geometry planar 3-DoF robot for stiffness synthesis purposes. This robot can change the geometry of its base platform to accommodate the required stiffness characteristics specific to each task. It has been shown, via polynomial formulation of the stiffness matrix in terms of the free geometry parameters, that for a given set of variable geometry parameters not all stiffness matrix terms are attainable, and a solution of the task-based stiffness synthesis problem through the use of Gröbner bases was presented.

In the present investigation we utilize the results of above-mentioned work for the stiffness synthesis of a 6-DoF robot composed of two variable geometry 3-DoF planar units. The aim of the synthesis is to obtain a specific stiffness for a given position/orientation of the robot's moving platform.

The following section of this work presents the architectures of the planar 3-DoF variable geometry units—one level out of two—that composes the DP 6-DoF robot. In Section 3

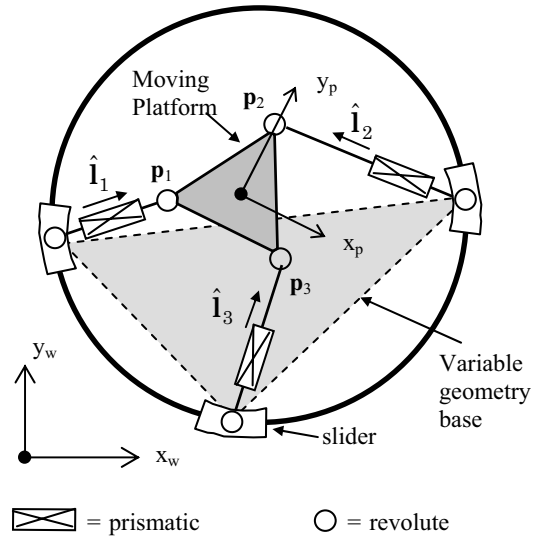


Fig. 1. Planar robot with variable geometry base.

we state the task-based stiffness synthesis problem. In Section 4 we decompose the stiffness of the DP robot in such a way as to allow the decomposition of the stiffness synthesis problem of the DP robot into two similar stiffness synthesis problems for each of its planar units. In Section 5 we present the solution algorithm for the stiffness synthesis problems of the 3-DoF planar units and the complete DP robot. In Section 6 we present a numerical example of the algorithm validating the theoretical results.

2. Variable Geometry 6-DoF Double Planar Robot

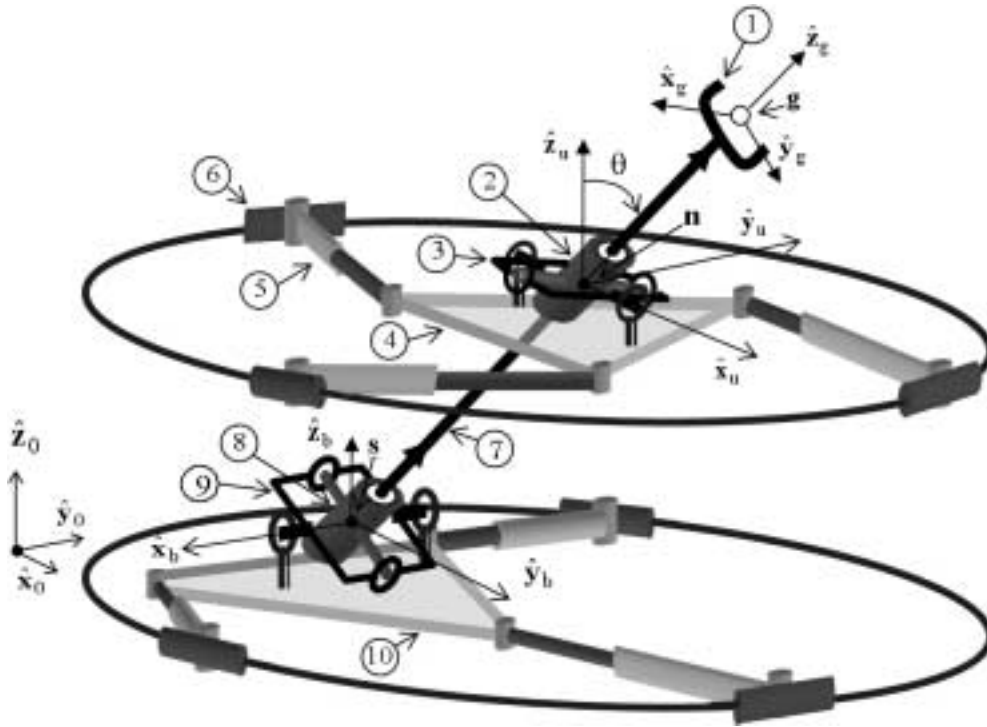
2.1. Variable Geometry Planar Robot

Figure 1 shows the variable geometry robot presented in Simaan and Shoham (2002) for stiffness synthesis. This robot has a triangular moving platform connected to a circular base by three kinematic chains composed of an active slider on the circular base, a passive revolute joint, an active prismatic joint, and another passive revolute joint on the moving platform.

The sliders on the circular base control the geometry of the base platform and the prismatic actuators are the active joints that manipulate the moving platform. This introduces a kinematic redundancy of three in this 3-DoF planar robot.

2.2. Variable Geometry Double Planar Robot

Figure 2 shows the variable geometry DP robot based on two similar planar units as in Figure 1. These planar units constitute a variation over the *Double Circular-Triangular* (DCT) robot presented in Simaan, Glozman, and Shoham (1998) and Brodsky, Glozman, and Shoham (1998), which, in its turn, is



| | | | |
|----------------------------|--------------------------------------|-----------------------------------|---|
| ① Gripper (end effector) | ⑦ Lead screw | s | Center point of the spline joint |
| ② Lead-screw nut | ⑧ Linear spline joint | $\hat{x}_0, \hat{y}_0, \hat{z}_0$ | World Coordinate System (WCS) |
| ③ Upper universal joint | ⑨ Lower universal joint | $\hat{x}_g, \hat{y}_g, \hat{z}_g$ | Gripper Coordinate System (GCS) |
| ④ Upper moving platform | ⑩ Lower moving platform | $\hat{x}_u, \hat{y}_u, \hat{z}_u$ | Upper platform-attached coordinate System |
| ⑤ Prismatic joint (active) | g Center point of the gripper | $\hat{x}_b, \hat{y}_b, \hat{z}_b$ | Lower platform-attached coordinate System |
| ⑥ Slider (active) | n Center point of the nut | χ | Universal joints' inclination angle |

Fig. 2. The DP variable geometry robot.

a variation over the *Double Triangular Robot* presented by Daniali, Zsombar-Murray, and Angeles (1993).

The two planar units of the DP robot control the position and orientation of their moving platforms by changing the lengths of their prismatic joints and the location of the sliders on their circular bases. In total, the DP robot has twelve controllable parameters: the six prismatic actuator lengths and the six locations of the sliders on their circular bases. All joints in this robot, other than the prismatic joints and the sliders on the circular bases, are passive joints.

The end effector of the DP robot is a gripper connected to a screw body that passes through the centers of the moving platforms of the planar units. The screw body mates with a nut

supported on a universal joint on the upper moving platform and passes through a passive linear spline coupling supported on a universal joint on the lower moving platform. Changing the planar positions of the upper and lower moving platforms controls the four DoFs of the line passing through their centers while controlling their rotations controls the displacement along the line and the orientation of the end effector about the line. The inverse kinematics of this robot is presented in detail in Appendix A.

The objective of this paper is to determine the locations of the six redundant sliders in order to achieve a desired stiffness goal for the DP robot.

3. Stiffness Synthesis with a Limited Number of Variable Geometry Parameters

Since in the DP robot only six parameters are redundant and their freedom lies in two planes, not any required stiffness is attainable. Stiffness synthesis with a limited number of variable geometry parameters, as in our case, calls for theoretical analysis that determines which terms of the stiffness matrix are controlled by the free geometrical parameters. In this paper the stiffness of the DP robot is formulated as a linear combination of the stiffnesses of its planar units. This allows us to decompose the stiffness synthesis problem of the DP robot into two similar stiffness synthesis problems dealing with finding the required locations of the sliders for each of the two planar units.

The stiffness matrices of the planar units are formulated (see Section 4) as polynomials in the free geometric variables; thus, different stiffness synthesis problems correspond to different systems of polynomials in these variables. The solubility of these polynomial systems was investigated in Simaan and Shoham (2002). This paper elaborates on the solution method and extends the solution procedure of the stiffness synthesis problem presented therein to the 6-DoF DP robot.

To solve the stiffness synthesis polynomial systems, the method of multiplication table eigenvalues (Stetter 1993) is used. This method was explained in Simaan and Shoham (2002) and it is briefly described in Appendix B. Further details of this method can be found in Möller and Stetter (1995) and Cox, Little, and O'Shea (1998).

4. Robot Stiffness Formulation

4.1. Polynomial Formulation for the Stiffness of the Planar Units

In this section, the stiffness matrices of the planar units of the DP robot are formulated as a function of the variable geometry parameters of its base platform, i.e., the slider positions on the circular bases. For any given desired gripper position and orientation, the inverse kinematics of the DP robot is solved and the corresponding positions and orientations of the planar units' moving platforms are found (see Appendix A). Once this solution is obtained, the only free geometric parameters that remain undetermined are the slider locations of the planar units. These locations are derived from stiffness synthesis requirements.

The unit vectors directions ($\hat{\mathbf{i}}_i, i=1, 2, 3$) along the prismatic actuator axes are the only free parameters that can be controlled by moving the sliders on the circular bases (Figure 1)

$$\hat{\mathbf{i}}_i = a_i \hat{\mathbf{e}}_1 + b_i \hat{\mathbf{e}}_2 \quad i = 1, 2, 3 \quad (1)$$

$$\hat{\mathbf{e}}_1 = [1, 0, 0]^T \quad \hat{\mathbf{e}}_2 = [0, 1, 0]^T$$

where the symbol \wedge indicates a unit vector, $\hat{\mathbf{e}}_1$ and $\hat{\mathbf{e}}_2$ are unit vectors along $\hat{\mathbf{x}}_w$ and $\hat{\mathbf{y}}_w$ respectively, $\hat{\mathbf{i}}_i$ is a unit vector along the i th prismatic actuator, and a_i, b_i are the projections of $\hat{\mathbf{i}}_i$ on $\hat{\mathbf{e}}_1$ and $\hat{\mathbf{e}}_2$. To make sure that the vector $\hat{\mathbf{i}}_i$ is a unit vector, the coordinates a_i and b_i ($i = 1, 2, 3$) must fulfill

$$a_i^2 + b_i^2 - 1 = 0. \quad (2)$$

The geometry of the moving platform used for this example approximates an equilateral triangle with a characteristic dimension h . The three revolute joints in the platform coordinate system (PCS), see Figure 1, are given by

$$\begin{aligned} \mathbf{P}_1 &= [-5h, -3h, 0]^T & \mathbf{P}_2 &= [0, 6h, 0]^T \\ \mathbf{P}_3 &= [5h, -3h, 0]^T. \end{aligned} \quad (3)$$

These vectors are transformed to the world coordinate system (WCS) by a rotation transformation, \mathbf{R} , given by the parameter t representing the tangent of half the moving platform's rotation angle:

$$\mathbf{R} = \begin{bmatrix} \frac{1-t^2}{1+t^2} & -2\frac{t}{1+t^2} & 0 \\ 2\frac{t}{1+t^2} & \frac{1-t^2}{1+t^2} & 0 \\ 0 & 0 & 1 \end{bmatrix}. \quad (4)$$

The Jacobian of the planar robot in Figure 1, with its sliders locked on the circular base, is given in eq. (5). The rows of this Jacobian are the Plücker line coordinates of the three axes of the prismatic actuators (Merlet 1989, 2000):

$$\begin{bmatrix} a_1 & b_1 & 0 & 0 & 0 & \left(10\frac{rh}{1+t^2} + \frac{3(1-t^2)h}{1+t^2}\right)a_1 \\ & & & & & + \left(-5\frac{(1-t^2)h}{1+t^2} + \frac{6rh}{1+t^2}\right)b_1 \\ a_2 & b_2 & 0 & 0 & 0 & -6\frac{(1-t^2)ha_2}{1+t^2} - \frac{12rhb_2}{1+t^2} \\ a_3 & b_3 & 0 & 0 & 0 & \left(-10\frac{rh}{1+t^2} + \frac{3(1-t^2)h}{1+t^2}\right)a_3 \\ & & & & & + \left(5\frac{(1-t^2)h}{1+t^2} + \frac{6rh}{1+t^2}\right)b_3 \end{bmatrix}. \quad (5)$$

Since in this paper we study the effect of stiffness modification/synthesis using a limited number of free geometric variables and a given set of actuators, we focus on the effect of geometry change instead of changing the stiffness coefficients of each actuator, as was done in previous works on stiffness control (Mason and Salisbury 1985). Accordingly, a simplifying assumption is made that the sliders on the circular

platform have a mechanical means to lock rigidly on the circular base once the desired geometry of the base is obtained or that the stiffness coefficients of the sliders are considerably larger than the stiffness coefficients of the prismatic actuators. The three active prismatic actuators are assumed to be identical, having stiffness coefficient k_d . This stiffness coefficient is either determined by the control law and transmission properties of each actuator or it is determined by the mechanical properties of the actuator for the case of non-back-drivable actuators. In this paper we assume non-back-drivable actuators with fixed stiffness coefficient, k_d , and that there is no preload on the robot. In accordance with all these assumptions, the 6×6 stiffness matrix is symmetric and is given by $\mathbf{K} = k_d \mathbf{J}^T \mathbf{J}$, (Gosselin 1990; Tsai 1999) and the reduced planar 3×3 stiffness matrix is then constructed by taking only the stiffness elements in the xx , xy , $x\theta$, yy , $y\theta$, and $\theta\theta$ directions.

4.2. Formulation of the Stiffness of the Double Planar Robot

In this section we combine the stiffness of the planar units to obtain the stiffness of the DP robot. This is used in Section 5 to determine which of the stiffness matrix elements can be controlled by the robot's redundant geometry variables.

Referring to Figure 2, the letters "s" and "n" indicate the center points of the spline joint and the nut, respectively, while the letter "g" represents the gripper center point and the letters "u" and "b" represent the upper and lower planar platforms.

Throughout this paper, the letters "v" and " ω " are used to indicate linear and angular velocities while the letters "s", "n", and "g", whenever used as subscripts, indicate a property associated with the linear spline, the nut and the gripper, respectively. Also, the letters "u" and "b" are used as subscripts to indicate properties associated with the upper and the lower moving platforms, respectively. Using this symbol convention, \mathbf{v}_s indicates the linear velocity of the spline center point, while $\boldsymbol{\omega}_g$ indicates the angular velocity vector of the gripper and ω_{gx} indicates the component of this vector along the x -axis of the WCS. The symbols $\dot{\mathbf{x}}_g$, $\dot{\mathbf{x}}_u$ and $\dot{\mathbf{x}}_b$ are respectively used to indicate the generalized velocities of the gripper and the upper and lower moving platforms of the planar units. These generalized velocities are defined in eqs. (6)–(8) (all vectors are column vectors expressed in the WCS unless otherwise specified):

$$\dot{\mathbf{x}}_g = [v_{gx}, v_{gy}, v_{gz}, \omega_{gx}, \omega_{gy}, \omega_{gz}]^T \quad (6)$$

$$\dot{\mathbf{x}}_u = [v_{ux}, v_{uy}, \dot{\theta}_u]^T \quad (7)$$

$$\dot{\mathbf{x}}_b = [v_{bx}, v_{by}, \dot{\theta}_b]^T \quad (8)$$

The actuator speeds of the upper planar platform and lower planar platform are respectively indicated by $\dot{\mathbf{q}}_u$ and $\dot{\mathbf{q}}_b$. These vectors are 3×1 vectors having the speeds of the active

prismatic actuators in Figure 1. The vector of actuator speeds for the DP robot is defined by $\dot{\mathbf{q}}$:

$$\dot{\mathbf{q}} = [\dot{\mathbf{q}}_u^T, \dot{\mathbf{q}}_b^T]^T \quad (9)$$

Using \mathbf{J} to denote the Jacobian of the DP parallel robot allows us to write its instantaneous inverse kinematics:

$$\dot{\mathbf{q}} = \mathbf{J} \dot{\mathbf{x}}_g \quad (10)$$

The instantaneous inverse kinematics of the upper and lower moving platforms are given by

$$\dot{\mathbf{q}}_b = \mathbf{J}_b \dot{\mathbf{x}}_b = \mathbf{J}_b \mathbf{A}_b \dot{\mathbf{x}}_g \quad \dot{\mathbf{q}}_u = \mathbf{J}_u \dot{\mathbf{x}}_u = \mathbf{J}_u \mathbf{A}_u \dot{\mathbf{x}}_g \quad (11)$$

where \mathbf{J}_b and \mathbf{J}_u are the Jacobians of the lower and upper planar units given in eq. (5) and \mathbf{A}_u and \mathbf{A}_b are 3×6 matrices to be formulated in the following subsection.

According to the definition in eqs. (9) and (10), the Jacobian of the DP robot is given by

$$\mathbf{J} = \begin{bmatrix} \mathbf{J}_u \mathbf{A}_u \\ \mathbf{J}_b \mathbf{A}_b \end{bmatrix} \quad (12)$$

Using the definition of the stiffness matrices of the planar units, we obtain the stiffness of the DP robot as a combination of the 3×3 reduced stiffness matrices, \mathbf{K}_u and \mathbf{K}_b , of the upper and lower planar units:

$$\mathbf{K} = k_d \mathbf{J}^T \mathbf{J} = \mathbf{A}_u^T \mathbf{K}_u \mathbf{A}_u + \mathbf{A}_b^T \mathbf{K}_b \mathbf{A}_b \quad (13)$$

4.3. Formulating \mathbf{A}_u and \mathbf{A}_b

The explicit expressions for matrices \mathbf{A}_u and \mathbf{A}_b in eq. (13) are formulated herein based on velocity constraint analysis of the planar units. These equations stem from the fact that the nut and the spline have no velocity component in the direction of $\hat{\mathbf{z}}_0$ (Figure 2), since they are constrained by the upper and lower moving platforms to planar motions.

Let r_{ij} ($i, j = 1, 2, 3$) indicate the elements of the rotation matrix from the gripper coordinate system (GCS) to the WCS. The unit vector $\hat{\mathbf{z}}_g$ in Figure 2 is given by the third column of this matrix, eq. (14), while $\hat{\mathbf{z}}_0$ is given by $[0, 0, 1]^T$:

$$\hat{\mathbf{z}}_g = [r_{13}, r_{23}, r_{33}]^T \quad (14)$$

We respectively define the vectors from the gripper center to the nut and spline center points as \mathbf{r}_{gn} and \mathbf{r}_{gs}

$$\mathbf{r}_{gs} = -l_s \hat{\mathbf{z}}_g \quad \mathbf{r}_{gn} = -l_n \hat{\mathbf{z}}_g \quad (15)$$

where l_n and l_s respectively indicate the distances between the gripper center and the center points of the nut and the linear spline.

Based on the generalized velocity, $\dot{\mathbf{x}}_g$, in eq. (6), the angular velocity matrix of the gripper is give by $\boldsymbol{\Omega}_g$:

$$\boldsymbol{\Omega}_g = \begin{bmatrix} 0 & -\omega_{gz} & \omega_{gy} \\ \omega_{gz} & 0 & -\omega_{gx} \\ -\omega_{gy} & \omega_{gx} & 0 \end{bmatrix} \quad (16)$$

The angular velocity of the linear spline, ω_s , is the same as the angular velocity of the gripper, ω_g , which is rigidly attached to the screw body (Figure 2):

$$\omega_s = \omega_g. \quad (17)$$

The projection of the angular velocity of the nut along the screw axis is indicated by a_n :

$$\omega_n^T \hat{z}_g = a_n. \quad (18)$$

Let the symbols v_{ng} and v_{sg} indicate the velocities of the nut and the spline relative to the gripper, which is rigidly attached to the screw. Also, let a_s indicate the speed of slip in the linear spline and let L be the lead of the screw (the amount of linear translation per turn of the screw relative to its nut). Using these definitions, v_{sg} is given by the slip speed a_s along the screw axis, \hat{z}_g , while the velocity of the nut relative to the gripper is given by the relative angular velocity of the nut about the screw times the lead of the screw:

$$v_{sg} = a_s \hat{z}_g \quad v_{ng} = [L(\omega_n - \omega_s)^T \hat{z}_g] \hat{z}_g. \quad (19)$$

Referring to Figure 2, the linear velocities of the spline and nut center points are given by the linear velocity of the gripper center point, the angular velocity matrix of the gripper, Ω_g , the corresponding relative slip velocity along the screw axis and their corresponding location with respect to the gripper center point:

$$\begin{aligned} v_s &= v_{sg} + v_g + \Omega_g r_{gs} \\ v_n &= v_{ng} + v_g + \Omega_g r_{gn}. \end{aligned} \quad (20)$$

Since both the linear spline and the nut are each supported on their corresponding universal joint (Figure 2), we need to consider the instantaneous kinematics of these joints in order to relate the angular velocity of their corresponding moving platform with their angular velocity about the screw axis. The instantaneous kinematics of these universal joints is given by

$$\dot{\theta}_b = f_b \dot{\theta}_s = f_b (\omega_g^T \hat{z}_g) \quad \dot{\theta}_u = f_u a_n. \quad (21)$$

The angular velocity transmission functions, f_u and f_b , of the U-joints, according to Wagner and Cooney (1979), are

$$\begin{aligned} f_u &= \frac{(1 - \sin^2(\beta_u) \sin^2(\theta))}{\cos(\theta)} \\ f_b &= \frac{(1 - \sin^2(\beta_b) \sin^2(\theta))}{\cos(\theta)} \end{aligned} \quad (22)$$

where θ is the universal joint angle (angle between \hat{z}_g and \hat{z}_0), and β_u and β_b are the angles from the axes of the upper and lower driving yokes to the normal to the plane defined by \hat{z}_g and \hat{z}_0 . Figure A3 (in Appendix A) shows the angle β_b ; the other angle β_u is defined similarly for the upper U-joint. The

driving yokes are rigidly connected to the moving platforms while the lower and upper driven yokes are, respectively, the spline body and the nut with their corresponding hinges (see Figures A3 and A4 in Appendix A).

Both the nut and spline center points are limited to perform planar motions. Accordingly, the velocity constraint equations used for finding the angular velocity component, a_n , of the nut and the sliding velocity of the spline joint, a_s , are given by

$$v_s^T \hat{z}_0 = 0 \quad v_n^T \hat{z}_0 = 0. \quad (23)$$

By using the formulation in eq. (20) and solving eq. (23) for a_n and a_s we obtain

$$\begin{aligned} a_n &= \frac{Lr_{33}\omega_{gx}r_{13} + Lr_{33}\omega_{gy}r_{23} + Lr_{33}^2\omega_{gz}}{Lr_{33}} \\ &\quad + \frac{-v_{gz} - \omega_{gy}l_n r_{13} + \omega_{gx}l_n r_{23}}{Lr_{33}} \end{aligned} \quad (24)$$

$$a_s = -\frac{v_{gz} + \omega_{gy}l_s r_{13} - \omega_{gx}l_s r_{23}}{r_{33}}. \quad (25)$$

Next these expressions for a_n and a_s are substituted in eqs. (19)–(21) and eqs. (7) and (8). Now \dot{x}_u and \dot{x}_b are expressed in terms of the elements of \dot{x}_g . Noticing the relations $\dot{x}_b = A_b \dot{x}_g$ and $\dot{x}_u = A_u \dot{x}_g$ in eq. (11), we obtain the expression for the elements of A_u and A_b by reading off the corresponding coefficients of the elements of \dot{x}_g . This results in the following expressions for A_u and A_b :

$$A_u = \begin{bmatrix} 1 & 0 & -\frac{r_{13}}{r_{33}} & \frac{r_{13}l_n r_{23}}{r_{33}} \\ 0 & 1 & -\frac{r_{23}}{r_{33}} & \frac{l_n r_{33}^2 + l_n r_{23}^2}{r_{33}} \\ 0 & 0 & -\frac{f_n}{Lr_{33}} & \frac{f_n(Lr_{33}r_{13} + l_n r_{23})}{Lr_{33}} \end{bmatrix} \quad (26)$$

$$A_b = \begin{bmatrix} 1 & 0 & -\frac{r_{13}}{r_{33}} & \frac{r_{13}l_s r_{23}}{r_{33}} \\ 0 & 1 & -\frac{r_{23}}{r_{33}} & \frac{l_s r_{33}^2 + l_s r_{23}^2}{r_{33}} \\ 0 & 0 & 0 & f_b r_{13} \end{bmatrix} \quad (27)$$

$$\begin{bmatrix} -\frac{l_s r_{33}^2 + l_s r_{13}^2}{r_{33}} & l_s r_{23} \\ -\frac{r_{13}l_s r_{23}}{r_{33}} & -l_s r_{13} \\ f_b r_{23} & f_b r_{33} \end{bmatrix}$$

Substituting \mathbf{A}_u and \mathbf{A}_b in eq. (13) yields the stiffness matrix of the DP robot in the WCS. The explicit expression for this matrix is not given for space considerations; however, one noticeable remark is in order regarding the characteristics of this matrix.

Huang and Schimmels (1998a) discussed the form of the stiffness matrix of a rigid body supported on simple linear or rotational springs and showed that, if the stiffness matrix is divided according to eq. (28), then it can be characterized by the nullification of the trace of its submatrix \mathbf{B} , eq. (29):

$$\mathbf{K} = \left\{ \begin{bmatrix} \mathbf{A} & \mathbf{B} \\ \mathbf{B}^T & \mathbf{C} \end{bmatrix} \in \mathbf{R}^{6 \times 6} : \mathbf{A} = \mathbf{A}^T, \mathbf{C} = \mathbf{C}^T, \mathbf{A}, \mathbf{C} \in \mathfrak{N}^{3 \times 3} \right\} \quad (28)$$

$$tr(\mathbf{K}\Delta) = 2tr(\mathbf{B}) = 0 \quad \Delta \equiv \begin{bmatrix} 0 & \mathbf{I} \\ \mathbf{I} & 0 \end{bmatrix}. \quad (29)$$

The condition in eq. (29) stems from the fact that the axes of simple linear springs are Plücker line coordinates fulfilling the *Klein quadric* condition (Pottman 1999). For the DP robot, the trace in eq. (29) has a distinct value given by

$$tr(\mathbf{K}\Delta) = 2tr(\mathbf{B}) = -2 \frac{f_u^2 K_{u_{\theta\theta}}}{L} \quad (30)$$

where $K_{u_{\theta\theta}}$ indicates the rotational stiffness of the upper planar unit, and L is the screw lead. This is an important characteristic of the DP robot since its architecture produces a screw spring acting on its gripper, although all its actuators are simple linear springs.

In the following section we present the solution of the stiffness synthesis problem for the DP robot based on the stiffness decomposition according to eq. (13). The desired stiffness characteristics of the DP robot are decomposed into two sets of desired stiffness characteristics for its planar units, and the slider locations are then calculated.

5. Stiffness Synthesis for the Double Planar Robot

5.1. General Description of the Synthesis Algorithm

Theoretically, it is possible to use a direct approach for the stiffness synthesis by using a polynomial formulation to the stiffness of the DP robot in terms of the locations of the six sliders of its planar units. This approach requires solving a system of twelve polynomials for twelve unknowns ($a_i, b_i, i = 1, 2, 3$ for each planar unit), in which six polynomials are in the form of eq. (2) and the other six are the equations for depicting the values of the six synthesized stiffness elements in the stiffness matrix. However, the polynomial systems associated with this approach are not practically solvable for the slider locations in the general case due to their size and

degree. Therefore, an indirect approach using the stiffness decomposition of eq. (13) is implemented. This stiffness decomposition gives the DP robot's stiffness matrix in terms of the stiffness matrices of its upper and lower planar units. Using this approach, the stiffness synthesis algorithm begins by decomposing the given stiffness synthesis problem into two simpler stiffness synthesis problems for the planar units and, later, these systems are solved separately.

In Section 5.2 we present the stiffness synthesis problems for the planar units. In Section 5.3 we present the solution to these stiffness synthesis problems and characterize the non-solvable stiffness synthesis problems for the given set of free geometric parameters, i.e., the slider locations. In Section 5.4 we present the method for decomposing the stiffness synthesis problems of the DP robot into two stiffness synthesis problems of its planar units.

5.2. Stiffness Synthesis for the Planar Units

Each planar 3-DoF unit has an associated 3×3 symmetric stiffness matrix (mentioned in Section 4.1) and the slider locations as three redundant parameters available for stiffness synthesis. Given a desired triplet of stiffness elements from the upper triangular part of the symmetric 3×3 stiffness matrix, the associated problem of stiffness synthesis is finding the required geometry of the base platform (i.e., finding $a_i, b_i, i = 1, 2, 3$) of the planar robot in Figure 1.

To fully synthesize the symmetric 3×3 stiffness matrix, all six equations in eq. (31) must be fulfilled together with the three equations in eq. (2). Since each planar mechanism of Figure 1 has a kinematic redundancy of order 3, only three stiffness equations from eq. (31) can be simultaneously fulfilled. Accordingly, there are $\binom{6}{3}=20$ systems of six polynomials with each having a total degree of 2 in $a_i, b_i (i = 1, 2, 3)$. Each of these systems represents a different stiffness synthesis problem in which a corresponding triplet of stiffness elements of the 3×3 stiffness matrix is being synthesized:

$$K_{ij} - K_{\text{desired},ij} = 0 \quad i = 1, 2, 3 \quad i \leq j. \quad (31)$$

Equation (31) poses the question whether it is possible to solve all the 20 stiffness synthesis problems, i.e., is changing the directions of the lines in Figure 1 enough to allow controlling all the stiffness triplets corresponding to the 20 stiffness synthesis problems?

5.3. Application of the Eigenvalue Method to the Planar Units

In this subsection we use the method of multiplication table eigenvalues given in Appendix B to solve the stiffness synthesis problem for the planar units. To answer the questions listed in the previous subsection, the reduced Gröbner bases associated with all the 20 possible systems of

equations in the form of eq. (31) were computed. A total-degree ordering (degree reverse lexicographical order) with $a_1 > b_1 > a_2 > b_2 > a_3 > b_3$ was used.

When the reduced Gröbner basis equals $\{1\}$, the system of polynomials has no solution (Adams and Loustanaou 1994). Hence, the use of Gröbner bases allows us to characterize the space of solvable synthesis problems of robots with a limited number of free geometric parameters. For the particular example of the planar units of the DP robot, it was found that whenever both k_{xx} and k_{yy} are specified then there is no solution to the system of polynomials (Simaan and Shoham 2002b). Physically, this means that with the free geometry parameters (slider locations) it is impossible to synthesize both k_{xx} and k_{yy} terms of the stiffness matrix.

To determine the solvability of the stiffness synthesis problems for the planar units, all 20 corresponding polynomial systems mentioned in Section 5.2 were symbolically formulated. These polynomial systems stem from eq. (31) for the corresponding triplets of synthesized stiffness elements and from eq. (2) for fulfilling the unit vector constraint on the lines of the Jacobian. Then, the corresponding reduced Gröbner bases for these polynomial systems were computed. All the non-solvable stiffness synthesis problems correspond to a reduced Gröbner basis $G = \{1\}$ since in this case the ideal is improper, i.e., $I = C[x_1 \dots x_m]$ where $C[x_1 \dots x_m]$ is the ring of polynomials with variables $x_1 \dots x_m$ and coefficients over the complex field C (Appendix B). Based on Hilbert's weak nullstellensatz theorem (Becker and Weispfenning 1993), an ideal has an empty variety $V(I)$ (i.e., empty solution set) if and only if $I = C[x_1 \dots x_m]$. Hence, by computing the reduced Gröbner bases and finding those that reduce to $\{1\}$ we find all the stiffness synthesis problems that are unsolvable.

Figure 3 gives a solvability map of all 20 possible stiffness synthesis problems mentioned in Section 5.1. Each tile represents an entry in the reduced 3×3 symmetric stiffness matrix of the planar unit. Light gray tiles indicate the synthesizable triplets while dark tiles indicate the non-synthesizable triplets of the stiffness matrix elements.

As an example, consider stiffness synthesis of k_{xx} , k_{xy} , and $k_{x\theta}$ elements of the stiffness matrix, i.e., all the stiffness elements in the x -direction are prescribed based on task requirements. The reduced Gröbner basis for this problem, hereafter called G , with total degree ordering $a_1 > b_1 > a_2 > b_2 > a_3 > b_3$ has 29 generators of degrees ranging from 1 to 5 in the free geometry variables. The symbolic computation of this particular basis took about 16 h using Maple on a 1Ghz Pentium III processor. The i th column in Table 1 presents the degrees of the i th basis polynomial in the variables corresponding to $a_1, b_1, a_2, b_2, a_3, b_3$. Table 1 shows that the total degree of the equations ranges from 4 to 8. Due to space considerations, this Gröbner basis is not presented here, but its leading terms are shown in eq. (32).

$$[a_3^2, a_2b_2, a_2^2, b_1^2, a_1b_1, a_1^2, b_1a_2a_3, a_2a_1a_3, b_2^3, b_2^2b_1, a_1b_2^2,$$

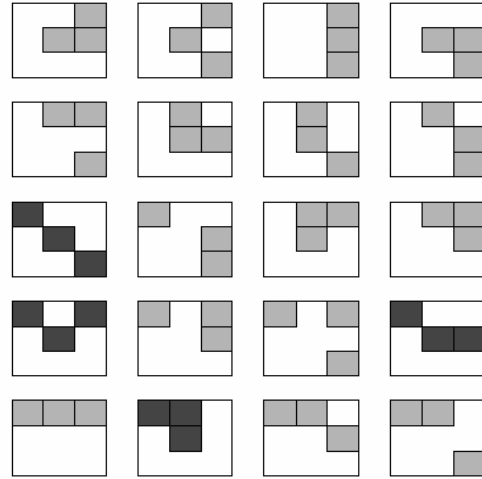


Fig. 3. Solvability map for the stiffness synthesis problems of the planar units.

$$\begin{aligned} & b_3^2b_2a_3, a_3b_3^2a_2, b_3^2b_1a_3, a_1b_3^2a_3, b_3^2b_2^2, b_1a_2b_3^2, b_3^2a_2a_1, \\ & b_3b_2^2a_3, b_1a_3b_2b_3, a_3b_2a_1b_3, b_3^5, b_3^4a_3, b_2b_3^4, a_2b_3^4, b_3^4b_1, \\ & b_3^4a_1, b_1b_2b_3^3, b_2b_3^3a_1]. \end{aligned} \quad (32)$$

Each variable among $\{a_1, b_1, a_2, b_2, a_3, b_3\}$ appears alone as a leading term in G with the corresponding degrees of $\{2, 2, 2, 3, 2, 5\}$, eq. (32). Consequently, based on the finiteness theorem (Adams and Loustanaou 1994), the system in eqs. (31) and (2) has a zero-dimensional variety. Also, the group of all the reminders in $C[a_1, b_1, a_2, b_2, a_3, b_3]/I$, denoted by D , has terms with maximal degrees of $\{1, 1, 1, 2, 1, 4\}$ in $\{a_1, b_1, a_2, b_2, a_3, b_3\}$, respectively. Hence, the monomial basis of $C[a_1, b_1, a_2, b_2, a_3, b_3]/I$, denoted by B , is found from D by extracting all the monomials in D that are equal to their own normal forms (Cox, Little, and O'Shea 1998). This procedure took 97 s to compute and resulted in the following 48-dimensional monomial basis:

$$\begin{aligned} & [1, b_3, a_3, b_2, a_2, b_1, a_1, b_3^2, b_3a_3, b_2b_3, a_2b_3, b_1b_3, a_1b_3, \\ & b_2a_3, a_2a_3, b_1a_3, a_1a_3, b_2^2, b_2b_1, b_2a_1, b_1a_2, a_2a_1, b_3^3, b_3^2a_3, \\ & b_3^2b_2, b_3^2a_2, b_1b_3^2, b_3^2a_1, a_3b_2b_3, a_2a_3b_3, b_1a_3b_3, a_3a_1b_3, \\ & b_3b_2^2, b_2b_1b_3, a_1b_2b_3, a_2b_1b_3, a_2a_1b_3, b_2^2a_3, b_2a_3b_1, \\ & a_1b_2a_3, b_3^4, a_3b_3^3, b_2b_3^3, a_2b_3^3, b_3^3b_1, b_3^3a_1, b_1b_2b_3^2, a_1b_2b_3^2]. \end{aligned} \quad (33)$$

To solve for the geometry free parameters (location of the sliders) three 48×48 multiplication tables, \mathbf{M}_{f_1} , \mathbf{M}_{f_2} and \mathbf{M}_{f_3} for $f_1 = a_1 + b_1$, $f_2 = a_2 + b_2$, and $f_3 = a_3 + b_3$, are computed together with their corresponding minimal polynomials, mp_{f_1} , mp_{f_2} , and mp_{f_3} . These minimal polynomials

Table 1. Degrees of the 29 Polynomials of G in the Variables

| | | | | | | | | | | | | | | | | | | | | | | | | | | | | | |
|-------|---|---|---|---|---|---|---|---|---|---|---|---|---|---|---|---|---|---|---|---|---|---|---|---|---|---|---|---|---|
| a_1 | 0 | 0 | 0 | 0 | 1 | 2 | 1 | 1 | 0 | 1 | 1 | 0 | 0 | 1 | 1 | 0 | 1 | 1 | 0 | 0 | 0 | 0 | 1 | 1 | 1 | 1 | | | |
| b_1 | 0 | 0 | 0 | 2 | 1 | 0 | 1 | 1 | 0 | 1 | 1 | 0 | 0 | 1 | 1 | 0 | 1 | 1 | 0 | 0 | 0 | 0 | 0 | 1 | 1 | 1 | 1 | | |
| a_2 | 0 | 1 | 2 | 0 | 0 | 0 | 1 | 1 | 1 | 0 | 0 | 1 | 1 | 0 | 0 | 1 | 1 | 0 | 1 | 1 | 0 | 0 | 1 | 1 | 0 | 0 | 1 | 1 | |
| b_2 | 0 | 2 | 2 | 2 | 2 | 2 | 1 | 1 | 3 | 2 | 2 | 1 | 1 | 0 | 0 | 2 | 1 | 1 | 2 | 1 | 1 | 2 | 2 | 1 | 1 | 0 | 0 | 1 | 1 |
| a_3 | 2 | 1 | 0 | 0 | 1 | 0 | 1 | 1 | 1 | 1 | 1 | 1 | 1 | 1 | 1 | 1 | 0 | 0 | 1 | 1 | 1 | 1 | 1 | 1 | 1 | 1 | 1 | 1 | |
| b_3 | 2 | 2 | 0 | 2 | 2 | 2 | 1 | 1 | 2 | 2 | 2 | 3 | 3 | 3 | 3 | 4 | 2 | 2 | 4 | 2 | 2 | 5 | 4 | 4 | 4 | 4 | 4 | 3 | 3 |

have only even degrees. Consequently, this stiffness synthesis problem has at most 24 pairs of complex solutions for f_1 , f_2 , f_3 and their conjugate solutions (48 solutions in total in terms of a_i , b_i , $i = 1, 2, 3$).

Once the sums $a_i + b_i$ ($i = 1, 2, 3$) are known, the values of a_1 , b_1 , a_2 , b_2 , a_3 , b_3 can be computed separately and the slider locations are found. The following is the solution procedure for (a_1, b_1) , which is identical for (a_2, b_2) , and (a_3, b_3) .

Let $\pm C$ be one of the solution pairs of mp_{f_1} . The corresponding solutions for (a_1, b_1) are given by solving

$$a_1 + b_1 = \pm C ; \quad a_1^2 + b_1^2 - 1 = 0. \quad (34)$$

The two solutions for $+C$ and two solutions for $-C$ are

$$\begin{aligned} \text{for } +C : (a_1, b_1) &= \left(\frac{C}{2} \pm \frac{\Delta}{2}, \frac{C}{2} \mp \frac{\Delta}{2} \right) \\ \text{for } -C : (a_1, b_1) &= - \left(\frac{C}{2} \mp \frac{\Delta}{2}, \frac{C}{2} \pm \frac{\Delta}{2} \right) \end{aligned} \quad (35)$$

$$\Delta \equiv \sqrt{2 - C^2}$$

Figure 4 shows the corresponding four solutions. The symbols Cp1, Cp2 indicate the two solutions in eq. (35) for $+C$ while Cm1, Cm2 designate the other two solutions for $-C$.

Note that each pair of solutions is a mirror image of the other about the unit vector $(\sqrt{2}/2, \sqrt{2}/2)$ with each solution forming an angle ξ according to

$$\xi = \cos^{-1} \left(\frac{C}{\sqrt{2}} \right). \quad (36)$$

Since only real solutions for (a_1, b_1) are of interest, only the real solution pairs of mp_{f_1} whose absolute values smaller than $\sqrt{2}$ are substituted in eq. (35) (see eq. (36)).

Once this procedure is repeated for the roots of mp_{f_2} and mp_{f_3} , sets of solutions for (a_2, b_2) and (a_3, b_3) are obtained. Then all sextuplets $(a_1, b_1, a_2, b_2, a_3, b_3)$ satisfying eqs. (31) are found; thus, determining the slider locations.

In this subsection we have presented a method to solve the stiffness synthesis of the planar units and to determine which combinations of the stiffness matrix terms are attainable. It was shown that for the robot of Figure 1, it is impossible to concurrently fulfill requirements of Cartesian stiffness matrix elements k_{xx} and k_{yy} by only changing the slider locations.

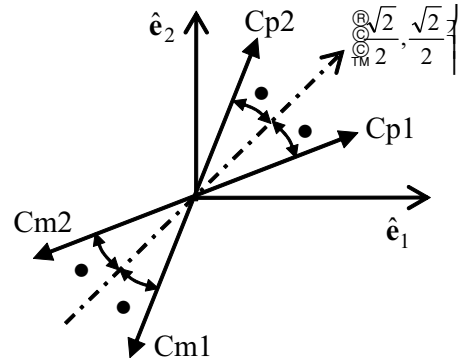


Fig. 4. Geometric interpretation to the solution in eq (39)

In the next subsection we solve the problem of task-based stiffness synthesis of the DP robot by using the results obtained from the stiffness synthesis of the variable geometry planar units.

5.4. Stiffness Synthesis for the Double Planar Robot

The stiffness synthesis problem of the 6-DoF DP robot is solved next. Given a desired sextuplet of stiffness parameters, we can solve linear equations stemming from eq. (13) for the desired stiffness elements of the planar units. Then, we have to solve two similar stiffness synthesis problems of the planar units by using the method of the previous section. Once the solutions for (a_i, b_i) , $i = 1..3$, are found for each planar unit, the slider locations are readily found.

To define solvability of all the stiffness synthesis problems for the DP robot, we have to compute all the corresponding Gröbner bases of all equations depicting sextuplets of stiffness elements. There are six redundant geometric variables in the DP robot and its 6×6 symmetric stiffness matrix has 20 independent variables since it is bound to fulfill eq. (30). This is tantamount to computing $\binom{20}{6}$ Gröbner bases, which is practically an impossible task. However, the stiffness of the DP robot is given according to eq. (13); therefore, synthesizing sextuplets of stiffness elements is limited only to those sextuplets that the planar units can attain. Accordingly, Fig-

ure 3 depicts the solvable synthesis problems for the planar units and also draws the limits for the solvable stiffness synthesis problems of the DP robot with the given redundancy. The unsolvable stiffness synthesis problems for the DP robot are all the stiffness synthesis problems for which one of the corresponding stiffness synthesis problems of its planar units is unsolvable according to Figure 3. Note also that eq. (13) is a linear combination of the two stiffness synthesis problems of the planar units, therefore the non-solvable stiffness synthesis problems for the DP robot are only those associated with non-solvable stiffness synthesis problems of one of its planar units.

The stiffness synthesis process for the DP robot is demonstrated herein for stiffness synthesis in the x -direction of the WCS. The solutions of the equations stemming from the stiffness decomposition equation (eq. (13)) for this problem are given by eqs. (37)–(42) where $[k_{x,x}, k_{x,y}, k_{x,z}, k_{x,\alpha}, k_{x,\beta}, k_{x,\gamma}]$ is the vector of desired (task-based) stiffness elements of the DP robot in the x -direction and \mathbf{K}_u and \mathbf{K}_b respectively designate the corresponding desired 3×3 stiffness matrices of the upper and lower planar units. Note that these equations show that this problem is solvable since eqs. (37)–(42) do not require simultaneously depicting $K_{u,x,x}$ and $K_{u,y,y}$ nor $K_{b,x,x}$ and $K_{b,y,y}$. In eqs. (37)–(42) r_{ij} , $i, j = 1, 2, 3$ indicate the elements of the rotation matrix \mathbf{R} from the GCS to the WCS:

$$K_{b_{x,x}} = \frac{l_n r_{13} K_{x,z} r_{33} + r_{23} K_{x,y} - K_{x,\beta} r_{33}}{-l_n + l_s} + \frac{r_{23} l_n r_{13} K_{x,y} + K_{x,\alpha} l_n r_{13}^2 - K_{x,x} l_n}{-l_n + l_s} \quad (37)$$

$$K_{b_{x,y}} = \frac{-l_n r_{33}^2 K_{x,y} + l_n r_{23} K_{x,z} r_{33} + r_{13} l_n r_{23} K_{x,x}}{-l_n + l_s} + \frac{K_{x,\alpha} r_{33} - r_{13} K_{x,y} - l_n r_{13}^2 K_{x,y}}{-l_n + l_s} \quad (38)$$

$$K_{b_{x,\theta}} = \frac{(K_{x,\beta} + L K_{x,y}) r_{23} + (K_{x,\gamma} + K_{x,z} L) r_{33}}{f_b} + \frac{(K_{x,\alpha} + L K_{x,x}) r_{13}}{f_b} \quad (39)$$

$$K_{u_{x,x}} = \frac{-l_n r_{13} K_{x,z} r_{33} - r_{23} K_{x,y} + K_{x,\beta} r_{33}}{-l_n + l_s} + \frac{-r_{23} l_n r_{13} K_{x,y} - K_{x,x} l_n r_{13}^2 + K_{x,x} l_s}{-l_n + l_s} \quad (40)$$

$$K_{u_{x,y}} = \frac{r_{13} K_{x,y} - K_{x,\alpha} r_{33} - r_{13} l_n r_{23} K_{x,x} - l_n r_{23} K_{x,z} r_{33}}{-l_n + l_s} + \frac{K_{x,y} l_s + l_n r_{13}^2 K_{x,y} + l_n r_{33}^2 K_{x,y} - l_n K_{x,y}}{-l_n + l_s} \quad (41)$$

$$K_{u_{x,\theta}} = \frac{-L r_{13} K_{x,x} - L r_{23} K_{x,y} - K_{x,z} L r_{33}}{f_n} \quad (42)$$

In the following section we demonstrate a numerical example of this algorithm.

6. Numerical Example: Stiffness Synthesis of the Double Planar Robot

In this section we demonstrate the solution of a stiffness synthesis problem for the DP robot of Figure 2. The unknowns are the locations of the sliders of the planar units. These locations are readily found once the solutions for the variables (a_i, b_i) , $i = 1..3$, are found for each planar unit of the DP robot. The aim of the synthesis problem is to specify all the six elements of the stiffness matrix in the x -direction of the WCS.

To validate the solution we first set up an example of the DP robot with given slider locations and compute its stiffness matrix according to eq. (13). The first row of this stiffness matrix (the stiffness elements in the x -direction) is used to set up the desired stiffness values for the stiffness synthesis algorithm. After solving for all possible solutions, the computed solutions are expected to include also the same values used for setting up the example.

6.1. Setting Up The Example

The geometric properties of the DP robot used for setting up the numerical example are listed in Table 2. The gripper of the robot is positioned in $\mathbf{g} = [-0.1, -0.1, 0.3]$ [m] and rotated 20° about the x -axis of the WCS.

The inverse kinematics given in Appendix A results in the rotation angles of the lower and upper moving platforms and in the positions of the spline and the nut together with the universal joint angles β_u and β_b (see Figure A3). The corresponding results for the required position and orientation of this example are given in Table 3.

Next, the angles of the prismatic actuator axes ($\hat{\mathbf{I}}_1, \hat{\mathbf{I}}_2, \hat{\mathbf{I}}_3$ in Figure 1) of the upper and lower planar units are selected as $\phi_u = [30^\circ, 240^\circ, 120^\circ]$ and $\phi_b = [60^\circ, 200^\circ, 100^\circ]$, respectively. The corresponding values for a_i, b_i , $i = 1, 2, 3$, are termed a_{u_i} and b_{u_i} for the upper planar unit and a_{b_i} and b_{b_i} for the lower planar unit:

$$\begin{aligned} \text{for upper planar unit: } & a_{u_i} = \cos(\phi_{u_i}) \\ & b_{u_i} = \sin(\phi_{u_i}) \\ \text{for lower planar unit: } & a_{b_i} = \cos(\phi_{b_i}) \\ & b_{b_i} = \sin(\phi_{b_i}) \\ & i = 1, 2, 3. \end{aligned} \quad (43)$$

The resulting reduced 3×3 stiffness matrices \mathbf{K}_u and \mathbf{K}_b for the upper and lower platforms are

Table 2. Numerical Parameters Used for Setting Up the Numerical Example

| | | | |
|--|------|--|-----------------|
| Upper platform height (Z_u in Figure A1) [m] | 0.2 | Characteristic dimension of lower moving platform [m] (see eq. (3)) | 0.02 |
| Homing height [m] | 0.3 | Characteristic dimension of upper moving platform [m] (see eq. (3)) | 0.02 |
| Radius of lower base circle [m] | 0.3 | Actuator stiffness of lower planar unit k_d [N m ⁻¹] | 1×10^5 |
| Radius of upper base circle [m] | 0.3 | Actuator stiffness of upper planar unit k_d [N m ⁻¹] | 1×10^5 |
| Screw lead (m per rotation) | 0.02 | | |

$$\mathbf{K}_u = \begin{bmatrix} 125000.0000 & 43301.27019 & 2495.777993 \\ 43301.27019 & 175000.0000 & -5084.097143 \\ 2495.777993 & -5084.097143 & 3924.257238 \end{bmatrix}$$

$$\mathbf{K}_b = \begin{bmatrix} 116317.5911 & 58339.64351 & -14955.57226 \\ 58339.64351 & 183682.4089 & -86.24677281 \\ -14955.57226 & -86.24677281 & 2367.426309 \end{bmatrix} \quad (44)$$

The resulting stiffness matrix of the DP robot is given by

$$\begin{bmatrix} 241317.5911 & 101640.9137 & 136598.9936 \\ 101640.9137 & 358682.4089 & -72352.98440 \\ 136598.9936 & -72352.98440 & .6150181290 \cdot 10^7 \\ 28349.51789 & 74837.93025 & 231755.2923 \\ -41639.92352 & -23106.75538 & 21805.93549 \\ -33063.17483 & -4443.898975 & -115627.0068 \\ 28349.51789 & -41639.92352 & -33063.17483 \\ 74837.93025 & -23106.75538 & -4443.898975 \\ 231755.2923 & 21805.93547 & -115627.0068 \\ 30053.33637 & -5474.412144 & -6114.035530 \\ -5474.412144 & 9056.655994 & 6604.974634 \\ -6114.035531 & 6604.974636 & 8789.449878 \end{bmatrix} \quad (45)$$

The elements of the first row of this stiffness matrix are selected as the desired values for the stiffness synthesis algorithm. Using the algorithm in Section 6.2, eqs. (37)–(42), results in the desired stiffness elements of the upper and lower units that are (as they should be) equal to the elements of the first rows of \mathbf{K}_u and \mathbf{K}_b of eq (45), respectively.

6.2. Solving for the Geometric Parameters of the Upper and Lower Platforms

The three desired stiffness elements for the upper and lower planar platforms that are given by the first rows of \mathbf{K}_u and \mathbf{K}_b ,

respectively, are used here as an input to the stiffness synthesis algorithm. For each planar unit, three minimal polynomials, mp_{f1} , mp_{f2} , and mp_{f3} , are obtained using the procedure of Section 5.3. Table 4 lists all distinct real solutions of mp_{f1} , mp_{f2} , and mp_{f3} for the upper and lower planar units.

Next, all the real solutions for a_i , b_i , $i = 1,2,3$ that are smaller than $\sqrt{2}$ are found by using eq. (34) (see eq. (36)). From these paired sets the sextuplets $[a_1, b_1, a_2, b_2, a_3, b_3]$ that fulfill the stiffness equations, of each planar unit, are saved. For the upper planar unit, this results in 48 real solutions for a_{u_i} , b_{u_i} , $i = 1,2,3$ while for the lower planar unit, eight real solutions for a_{b_i} , b_{b_i} , $i = 1,2,3$ are found. Figures 5 and 6 present the geometry of the upper and lower planar units for the solutions given numerically in Appendix C. The three actuators in Figure 1 are distinguished in these figures by circular, hexagram, and square symbols, respectively. The solutions corresponding to the angles used to set up the example are encircled. The time for the numerical computation of the eigenvalues took about 500 s for each planar unit.

Appendix C presents all real solutions for the upper and lower planar units, respectively. All computations were carried out with 64 digit accuracy. The values for $[a_1, b_1, a_2, b_2, a_3, b_3]$ are presented as angles of the prismatic actuators in Appendix C (\hat{I}_i , $i = 1,2,3$ in Figure 1) in the x - y plane. Any solution for the upper planar unit can be used with any solution for the lower planar units; hence Appendix C presents all 384 real solutions for the stiffness synthesis problem of the DP robot of this example. Highlighted rows in Appendix C represent the solutions corresponding to the values of the actuator angles used for setting up the numerical example.

7. Conclusions

A solution for the stiffness synthesis problem of DP variable geometry parallel robots is presented in this investigation. This solution uses Gröbner bases and applies multiplication tables that transform the solution of the stiffness synthesis polynomial equations into an eigenvalue problem. Since in

Table 3. Results of the Inverse Kinematics of the Double Planar Robot

| | | | |
|--|---------------------------|---|-------------------|
| \mathbf{n} = position of the nut | $[-0.1, -0.0636, 0.20]^T$ | β_b = lower U-joint angle (see Figure A3 in Appendix A) | 0.0 |
| \mathbf{s} = position of the spline | $[-0.1, 0.0092, 0.0]^T$ | β_u = upper U-joint angle (see Figure A3 in Appendix A) | -65.8384° |
| θ_b = rotation of lower moving platform | 0.0° | θ_{sn} = relative rotation between screw and nut | -115.5120° |
| θ_u = upper moving platform rotation | -114.1616° | | |

The number of four digits after the decimal points is only for numerical purposes.

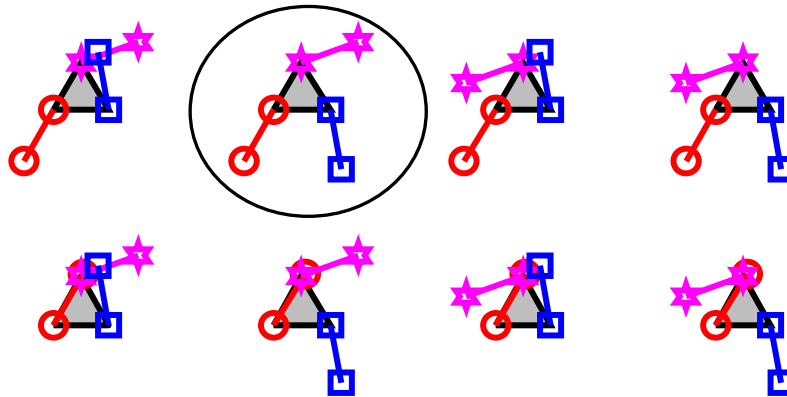


Fig. 5. Geometry of the lower planar unit for all eight solutions of the stiffness synthesis example of the DP robot. The encircled solution corresponds to the data used for setting up the numerical example.

Table 4. Real Solutions of mp_{f1} , mp_{f2} , and mp_{f3} for the Upper Planar Unit and Lower Planar Unit

| Results for Upper Planar Unit | | | Results for Lower Planar Unit | | |
|-------------------------------|------------------|------------------|-------------------------------|------------------|------------------|
| C_1 | C_2 | C_3 | C_1 | C_2 | C_3 |
| ± 0.20894173 | ± 0.96642204 | ± 0.36602540 | ± 1.3636051 | ± 0.29022483 | ± 0.81115957 |
| ± 0.22517095 | ± 1.0048748 | ± 0.56625616 | | ± 1.1215331 | ± 0.8328858 |
| ± 0.99510127 | ± 1.0509660 | ± 0.94629300 | | ± 1.2703051 | ± 1.1445878 |
| ± 1.3659867 | ± 1.3660254 | ± 1.0324865 | | ± 1.2817127 | ± 1.3356068 |
| ± 1.3660254 | ± 1.3926714 | ± 1.2881221 | | ± 1.3525921 | ± 1.3615997 |
| | ± 1.3986934 | ± 1.3613936 | | | |
| | ± 1.4003424 | ± 1.3660254 | | | |
| | | ± 1.3961726 | | | |

All numerical computations in this work were made with 64 digits, but results are truncated to eight significant decimal digits for presentation purposes.

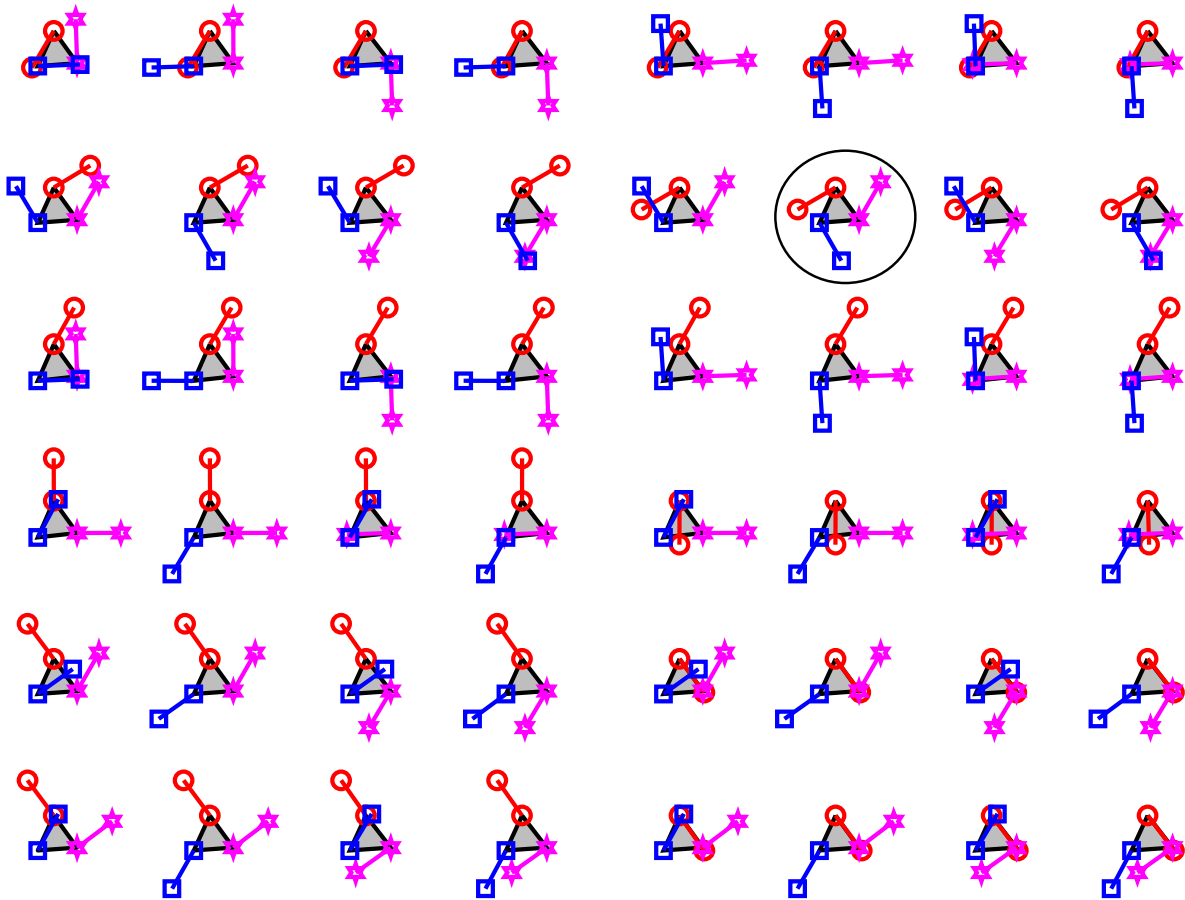


Fig. 6. Geometry of the upper planar unit for all 48 solutions of the stiffness synthesis example of the DP robot. The encircled solution corresponds to the data used for setting up the numerical example.

practice the number of actuators is deficient for synthesizing the complete stiffness matrix, we take advantage of Gröbner bases to characterize the space of solvable stiffness synthesis problems for a given set of variable geometry parameters. The effectiveness of this method was demonstrated on a novel DP variable geometry robot which has six free geometry variables and can control at most six elements of its stiffness matrix.

Due to the special structure of the DP robot it is possible to decompose the problem into two stiffness synthesis problems of its upper and lower planar platforms that have three free geometry variables each. The solution of the stiffness synthesis of the planar units was shown to have at most 48 solutions. For each planar unit it was shown, for example, that it is impossible to control both two elements, K_{xx} and K_{yy} , of the stiffness matrix by only changing the locations of the sliders on the circular base. Composing the solvable sets of elements of the stiffness matrix of the planar units draws the limits of the solvable sets of the stiffness matrix elements for the 6-DoF DP robot. This method was verified by an example

that synthesizes the stiffness matrix elements of the DP robot in the X -direction that was shown to have 384 real solutions.

Appendix A: Inverse Kinematics of the Double Planar Robot

Figure A1 shows a schematic view of the gripper in four positions. The upright position of the screw body is considered the *home position* (position 1 in Figure A1). In this position, the moving platforms of the two planar units are at the centers of their circular bases and their PCS are parallel to the WCS. The fourth position represents a general position of the gripper. Subscript h in Figure A1 indicates all the properties at the home position and the letters g , n , s respectively indicate the positions of the gripper, the nut, and the spline center points in the WCS.

To reach any desired configuration from the home position, the motion is conceptually decomposed into three parts.

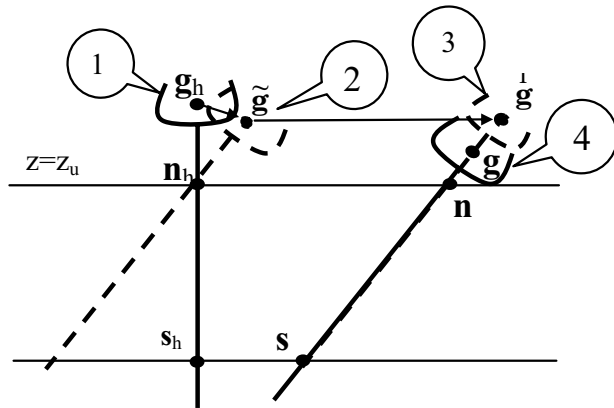


Fig. A1. Motion from the home position to a general given position.

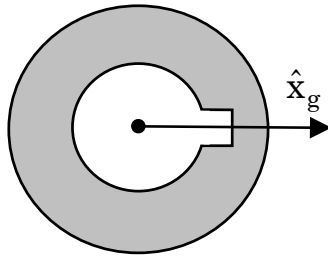


Fig. A2. Cross-section of the spline joint.

The first part (transition from position 1 to position 2) is rotation about the center point of the nut at home position, n_h in Figure A1, such that the desired orientation of the gripper is reached and the corresponding rotation of the lower platform is determined by the inverse kinematics of the lower U-joint (eq. (A3)). To maintain the axial position of the screw body relative to the nut, the upper moving platform is rotated in the same amount as the lower moving platform. Next, parallel translation of both the upper and lower moving platforms is performed until the desired position of the screw axis is obtained (position 3, Figure A1). Finally, only the upper moving platform is rotated in order to move the end effector axially on the screw to the desired axial position (position 4, Figure A1).

Apart from the GCS and WCS, we introduce an upper PCS, lower PCS, and nut-attached coordinate system (NCS). The details of these systems are given in Figures A2–A4 and are explained in the subsequent paragraphs. At the home position all these coordinate systems are parallel to the WCS.

Let the symbol \wedge indicate a unit vector. Accordingly, let \hat{z}_g and \hat{z}_0 indicate the unit vectors along the screw axis and the

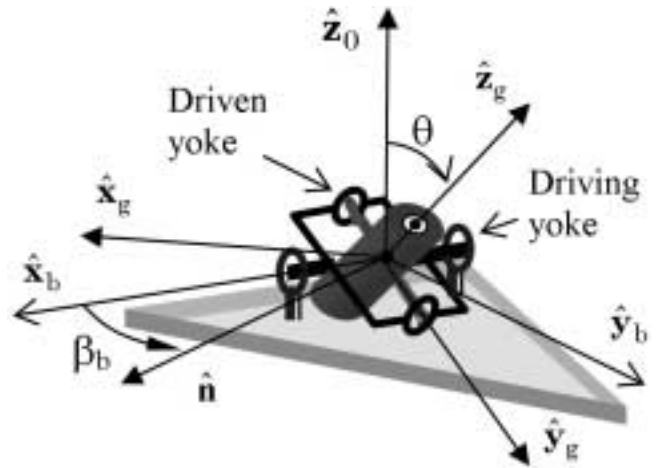


Fig. A3. Lower moving platform, universal joint and spline.

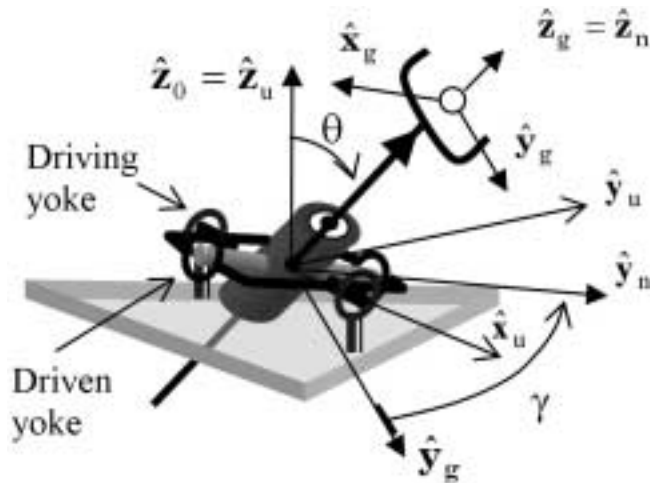


Fig. A4. Upper moving platform, universal joint, screw body and gripper.

z -direction of the WCS (see Figure 2) respectively. \hat{z}_g is given by the third column of wR_g , the rotation matrix from the GCS to WCS. The parametric locus of all points along the screw axis is indicated by \mathbf{l} in eq. (A1) where $\zeta \in \mathfrak{R}$ is the position parameter along the screw axis:

$$\mathbf{l} = \mathbf{g} - \zeta \hat{z}_g. \tag{A1}$$

The nut and spline center points (points \mathbf{n} and \mathbf{s}) are found by substituting in eq. (A1) $z = z_u$ and $z = 0$, respectively:

$$\mathbf{s} = \mathbf{g} - \begin{pmatrix} \mathbf{g}^T \hat{z}_0 \\ \hat{z}_g^T \hat{z}_0 \end{pmatrix} \hat{z}_g \quad \mathbf{n} = \mathbf{g} - \begin{pmatrix} \mathbf{g}^T \hat{z}_0 - z_u \\ \hat{z}_g^T \hat{z}_0 \end{pmatrix} \hat{z}_g. \tag{A2}$$

Figure A2 introduces the geometry of the spline supported by the lower U-joint. The direction from the center point to

the groove of the spline is parallel to $\hat{\mathbf{x}}_g$, the x -direction of the GCS (Figures A1 and A2). Figure A3 gives the geometry of the U-joint connecting the spline to the lower platform. The “driving yoke” of this universal joint is rigidly connected to the lower moving platform and the lower PCS is indicated by subscript b such that its x -direction, $\hat{\mathbf{x}}_b$, is along the pivot of the driving yoke and its z -direction is always parallel to $\hat{\mathbf{z}}_0$ (Figure A3). The driven yoke of this U-joint is the spline with its hinge always parallel to $\hat{\mathbf{y}}_g$, the y -direction of the GCS. The geometry of the upper U-joint fixed to the upper moving platform is identical when the spline of the lower U-joint is replaced with the nut of the upper joint. However, since the nut can rotate about the screw, the NCS is defined with its z -direction along $\hat{\mathbf{z}}_g$ and y -direction perpendicular to $\hat{\mathbf{z}}_g$ and along the axis of the driven yoke (see $\hat{\mathbf{z}}_n$ and $\hat{\mathbf{y}}_n$ in Figure A4). The x -direction of the upper PCS, $\hat{\mathbf{x}}_u$, is along the pivot of the driving yoke connected to the upper moving platform.

The angle between $\hat{\mathbf{z}}_0$ and $\hat{\mathbf{z}}_g$ is labeled θ (Figures A3 and A4). The rotation angle of the lower moving platform relative to the home position is given by the direction of $\hat{\mathbf{x}}_b$ in the $\hat{\mathbf{x}}_0 - \hat{\mathbf{y}}_0$ plane. Since the structure of the U-joint depicts perpendicularity of $\hat{\mathbf{y}}_g$ to $\hat{\mathbf{x}}_b$, the direction of $\hat{\mathbf{x}}_b$ is given by

$$\theta_b = \text{Atan2}(y_{b2}/y_{b1}) - \pi/2, \quad (\text{A3})$$

where (y_{b1}, y_{b2}) indicate the projections of $\hat{\mathbf{y}}_g$ on the $\hat{\mathbf{x}}_0 - \hat{\mathbf{y}}_0$ plane. This solution is one of two possible solutions to the inverse kinematics of the U-joint and it corresponds to the geometry in Figure A3.

Once the lower and upper moving platforms are rotated by θ_b and translated to points \mathbf{n} and \mathbf{s} given by eq. (A2), the desired orientation of the gripper is achieved such that the desired gripper position, \mathbf{g} , lies along $\hat{\mathbf{z}}_g$. In this position, homothetic edges of the upper and lower platforms are parallel and $\hat{\mathbf{y}}_n$ is parallel to $\hat{\mathbf{y}}_g$. To achieve the desired position, \mathbf{g} , what remains is rotating only the upper moving platform (and thus the nut about the screw) in order to produce the desired axial motion, a_m , of the screw relative to the nut. The axial motion is given by

$$a_m = \|\mathbf{g} - \mathbf{n}\| - \|\mathbf{g}_h - \mathbf{n}_h\|. \quad (\text{A4})$$

Since the axial motion, a_m , is achieved by rotating the nut and not the screw, the corresponding required rotation angle of the nut about $\hat{\mathbf{z}}_g$, is given by

$$\theta_{sn} = -2\pi (a_m/L) (a_m/|a_m|) \quad (\text{A5})$$

where L indicates the lead of the right-handed screw thread in mm per revolution.

Rotating $\hat{\mathbf{y}}_g$ about $\hat{\mathbf{z}}_g$ in an angle of $\gamma = \theta_{sn}$, defines $\hat{\mathbf{y}}_n$ corresponding to the desired orientation of the nut

$$\hat{\mathbf{y}}_n = {}^w\mathbf{R}_g\mathbf{R}_{z_g,\gamma}[0, 1, 0]^T \quad (\text{A6})$$

where $\mathbf{R}_{z_g,\gamma}$ is the rotation matrix by an angle γ about $\hat{\mathbf{z}}_g$:

$$\mathbf{R}_{z_g,\gamma} = \begin{bmatrix} c_\gamma & -s_\gamma & 0 \\ s_\gamma & c_\gamma & 0 \\ 0 & 0 & 1 \end{bmatrix}. \quad (\text{A7})$$

The unit vector $\hat{\mathbf{y}}_u$ is obtained by normalizing the vector produced by projecting $\hat{\mathbf{y}}_n$ on the $x_0 - y_0$ plane and $\hat{\mathbf{x}}_u$ is found from the cross product of $\hat{\mathbf{y}}_u$ with $\hat{\mathbf{z}}_0$. The directed angle from $\hat{\mathbf{x}}_b$ to $\hat{\mathbf{x}}_u$ is given by

$$\alpha = \text{Atan2}(\hat{\mathbf{x}}_u^T\hat{\mathbf{y}}_b, \hat{\mathbf{x}}_u^T\hat{\mathbf{x}}_b) \quad \alpha \in [0, 2\pi). \quad (\text{A8})$$

Let n_r indicate the number of complete revolutions made by the screw relative to the nut. The total rotation angle θ_u of the moving platform relative to its orientation at the home position is given by eq. (A9) and explained in Figure A5

$$\theta_u = \theta_b - (2\pi n_r + \beta)\text{sign}(a_m) \quad (\text{A9})$$

where β is related to α and the sign of a_m :

$$\beta = \pi(\text{sign}(a_m) + 1) - \text{sign}(a_m)\alpha. \quad (\text{A10})$$

Equations (A2), (A3) and (A9) complete the inverse position analysis of the DP robot.

Appendix B: The Eigenvalue Method for Solving Polynomial Systems

Let $C[x_1 \dots x_m]$ represent the *ring* of polynomials with variables $x_1 \dots x_m$, and coefficients over the complex field, C . Let also $S = \{p_1, p_2, \dots, p_n | p_1, p_2, \dots, p_n \in C[x_1 \dots x_m]\}$ be a system of n polynomials with a corresponding zero-dimensional Ideal $I = \langle p_1, p_2, \dots, p_n \rangle$, $I \subset C[x_1 \dots x_m]$. The *variety* $V(I)$ of solution is defined by all the m -tuples of $x_1 \dots x_m$ such that $p_1 = p_2 = \dots = p_n = 0$, i.e., $V(I) = \{[x_1 \dots x_m] \in C^m | p_1 = p_2 = \dots = p_n = 0\}$. We seek all the solutions of S .

The original system of polynomial equations, S , can be replaced by another minimal set of polynomials, $G = \{g_1 \dots g_t\}$, called *standard basis* (or *Gröbner basis*) of the ideal I via the use of Buchberger’s algorithm (Buchberger 1965), which is not reviewed here due to lack of space. Questions regarding ideal-membership of a given polynomial to I , solubility of S , and finiteness of the dimension of $V(I)$ are readily answered when using this basis (Heck 1997). Also, if G is computed with a lexicographic ordering, it results in a system of polynomials with a consecutively eliminated number of variables as in the result of the Gauss–Jordan elimination method for linear equations. However, this elimination method is unfavorable for large systems because of the computation effort associated with this ordering (Cox, Little, and O’Shea 1998).

It is said that two polynomials f and g , $f, g \in C[x_1 \dots x_m]$, are *congruent*, $f \equiv g \pmod{I}$, if $f-g \in I$. In such a case

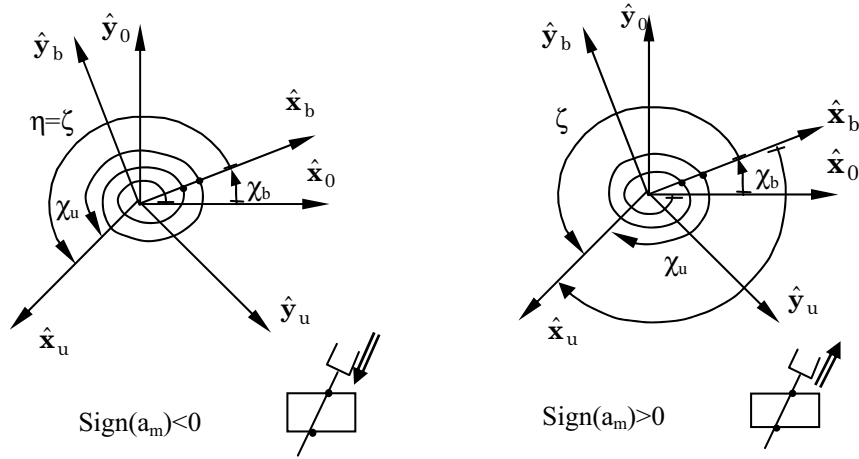


Fig. A5. Relations between β , α , θ_u , and θ_b for $\text{sign}(a_m) = \pm 1$.

they have the same *normal form* when reduced with respect to G and, therefore, are associated with equal cosets $[g] = [f]$. A coset $[f]$ of a polynomial $f \in C[x_1..x_m]$ is defined as the subgroup of $C[x_1..x_m]$ in which all its elements have the same normal form with respect to G , $[f] = f + I = \{f + h | h \in I\}$. The totality of cosets of the polynomials in $C[x_1..x_m]$ is the quotient ring of $C[x_1..x_m]$ modulo I indicated by $C[x_1..x_m]/I$, i.e., $C[x_1..x_m]/I = \{f + I | f \in C[x_1..x_m]\}$.

The definition of a coset of a polynomial $f \in C[x_1, \dots, x_m]$ associates f with the coset of all polynomials in $C[x_1, \dots, x_m]$ having the same normal form with respect to an ideal I . One interesting property of normal forms is that the normal form of any polynomial $f \in C[x_1, \dots, x_m]$ is always a complex combination of monomials over $C[x_1, \dots, x_m]$. These monomials are called the *basis monomials* (Cox, Little, and O'Shea 1998) or, simply, the *monomial basis* and are indicated by $B = \{b_1, \dots, b_s\}$. This means that the normal form of every polynomial in $C[x_1, \dots, x_m]$ is given by the complex combination $\sum_{i=1}^s c_i b_i$ where $c_i \in C$ and $b_i \in B$. This is expressed by the congruence relation in the following equation:

$$f \equiv \sum_{i=1}^s c_i b_i \pmod{I} \quad | \quad c_i \in C, b_i \in B$$

$$\forall f \in C[x_1, \dots, x_m]. \tag{B1}$$

Consider now another polynomial $p \in C[x_1, \dots, x_m]$ and define the following linear mapping of cosets:

$$\Psi_p : C[x_1, \dots, x_m]/I \rightarrow C[x_1, \dots, x_m]/I,$$

$$\Psi_p([f]) = [pf], \quad p, f \in C[x_1, \dots, x_m]. \tag{B2}$$

This mapping constitutes an endomorphism (Möller 1998), and has a matrix representation and eigenvalues.

To define this matrix representation, we recall the monomial basis B for $C[x_1, \dots, x_m]/I$ and we define for each polynomial $f \in C[x_1, \dots, x_m]$ a multiplication table, \mathbf{M}_f , as given in the following definition.

DEFINITION 1. *Multiplication table* Let I be an ideal over $C[x_1, \dots, x_m]$, G its Gröbner basis, and $\mathbf{b} = [b_1, \dots, b_s]^T$ be a vector of the monomial basis elements of its quotient ring $C[x_1, \dots, x_m]/I$. Every polynomial $f \in C[x_1, \dots, x_m]$ has an associated multiplication table \mathbf{M}_f such that

$$f \mathbf{b} \equiv \mathbf{M}_f \mathbf{b} \pmod{I}. \tag{B3}$$

From the above definition, it is possible to write the normal form with respect to the Gröbner basis G of $f b_i$ for each element of the monomial basis, $b_i, i = 1 \dots s$, as a combination of the monomial basis elements in B :

$$n_f(f b_i) = \sum_{i=1}^s c_i b_i \quad | \quad c_i \in C, b_i \in B. \tag{B4}$$

Equation (B4) defines the i th column of the matrix \mathbf{M}_f as the vector of coefficients $\mathbf{c} = [c_1, \dots, c_s]^T$.

The key point behind the method of the multiplication table eigenvalues is eq. (B3), which implies the following

$$f \mathbf{b} - \mathbf{M}_f \mathbf{b} \in I. \tag{B5}$$

Therefore, for all the points, $\mathbf{a} \in V(I)$, of the solution set $V(I)$, all polynomials in I vanish; hence we can write

$$f \mathbf{b} - \mathbf{M}_f \mathbf{b} = \mathbf{0} \quad \forall \mathbf{a} \in V(I). \tag{B6}$$

Equation (B6) indicates that, for all the points $\mathbf{a} \in V(I)$, when substituting these points in f and in the vector of monomial basis elements, \mathbf{b} , all s equations in eq. (B6) vanish simultaneously. This defines the eigenvalue problem:

$$(\mathbf{M}_f - f \mathbf{I}) \mathbf{b} = \mathbf{0}. \tag{B7}$$

Table C-1: All 48 real solutions for prismatic actuators' angles $\lambda_1, \lambda_2, \lambda_3$ of the upper planar unit

| | | | | | | | | |
|-------------|-------------|-------------|-------------|-------------|-------------|-------------|-------------|-------------|
| 306.5037827 | 216.5037827 | 240.0000000 | 270.2799935 | 180.2799936 | 240.0000000 | 210.0000001 | 240.0000000 | 300.0000000 |
| 306.5037827 | 216.5037827 | 59.99999998 | 270.2799935 | 180.2799936 | 59.99999998 | 210.0000001 | 240.0000000 | 120.0000000 |
| 306.5037827 | 36.50378270 | 240.0000000 | 270.2799935 | .2799934890 | 240.0000000 | 210.0000001 | 59.99999998 | 300.0000000 |
| 306.5037827 | 36.50378270 | 59.99999998 | 270.2799935 | .2799934890 | 59.99999998 | 210.0000001 | 59.99999998 | 120.0000000 |
| 126.5037826 | 216.5037827 | 240.0000000 | 90.27999346 | 180.2799936 | 240.0000000 | 29.99999999 | 240.0000000 | 300.0000000 |
| 126.5037826 | 216.5037827 | 59.99999998 | 90.27999346 | 180.2799936 | 59.99999998 | 29.99999999 | 240.0000000 | 120.0000000 |
| 126.5037826 | 36.50378270 | 240.0000000 | 90.27999346 | .2799934890 | 240.0000000 | 29.99999999 | 59.99999998 | 300.0000000 |
| 126.5037826 | 36.50378270 | 59.99999998 | 90.27999346 | .2799934890 | 59.99999998 | 29.99999999 | 59.99999998 | 120.0000000 |
| 305.8383803 | 240.0000000 | 215.8383803 | 240.0000000 | 271.8929528 | 181.8929528 | 59.99999998 | 271.8929528 | 181.8929528 |
| 305.8383803 | 240.0000000 | 35.83838027 | 240.0000000 | 271.8929528 | 1.892952769 | 59.99999998 | 271.8929528 | 1.892952769 |
| 305.8383803 | 59.99999998 | 215.8383803 | 240.0000000 | 91.89295273 | 181.8929528 | 59.99999998 | 91.89295273 | 181.8929528 |
| 305.8383803 | 59.99999998 | 35.83838027 | 240.0000000 | 91.89295273 | 1.892952769 | 59.99999998 | 91.89295273 | 1.892952769 |
| 125.8383802 | 240.0000000 | 215.8383803 | 240.0000000 | 183.0000317 | 273.0000316 | 59.99999998 | 183.0000317 | 273.0000316 |
| 125.8383802 | 240.0000000 | 35.83838027 | 240.0000000 | 183.0000317 | 93.00003159 | 59.99999998 | 183.0000317 | 93.00003159 |
| 125.8383802 | 59.99999998 | 215.8383803 | 240.0000000 | 3.000031618 | 273.0000316 | 59.99999998 | 3.000031618 | 273.0000316 |
| 125.8383802 | 59.99999998 | 35.83838027 | 240.0000000 | 3.000031618 | 93.00003159 | 59.99999998 | 3.000031618 | 93.00003159 |

All 8 real solutions for prismatic actuators' angles $\lambda_1, \lambda_2, \lambda_3$ of the lower planar unit

| | | | | | |
|-------------|-------------|-------------|-------------|-------------|-------------|
| 240.0000000 | 200.0000001 | 280.0000000 | 59.99999998 | 200.0000001 | 280.0000000 |
| 240.0000000 | 200.0000001 | 99.99999999 | 59.99999998 | 200.0000001 | 99.99999999 |
| 240.0000000 | 19.99999999 | 280.0000000 | 59.99999998 | 19.99999999 | 280.0000000 |
| 240.0000000 | 19.99999999 | 99.99999999 | 59.99999998 | 19.99999999 | 99.99999999 |

Equation (B7) is the basis for the method of multiplication table eigenvalues in the following theorem (Cox, Little, and O'Shea 1998).

THEOREM 1. Let $I \subset C[x_1, \dots, x_m]$ be a zero-dimensional ideal. Let $f \in C[x_1, \dots, x_m]$ and \mathbf{M}_f its corresponding multiplication table in $C[x_1, \dots, x_n]/I$. The eigenvalues of \mathbf{M}_f are the corresponding values of f for all the points of $V(I)$.

Theorem 1 defines the basic form for the method of multiplication table eigenvalues. Accordingly, in order to solve a polynomial system in $C[x_1, \dots, x_m]$ we have to compute all multiplication tables \mathbf{M}_f where $f = x_i, i = 1, 2, \dots, m$, and find all their eigenvalues. Then by substituting in the polynomial system it is possible to find all the solution vectors in $V(I)$.

This method has several advantages over standard sequential elimination by resultants mentioned in Raghavan and Roth (1995) and Neilsen and Roth (1999). The numerical compu-

tation is kept to a minimum by using it only for eigenvalue computation. Also, unlike sequential elimination, the solution of each variable x_i is independent of the other variables x_j and, thus, it is unaffected by computation errors in x_j . Additionally, by using Gröbner bases the solvability of the system of polynomial equations is determined and it is unaffected by the term order used for the computation of G , which allows using more efficient term orders such as total degree order (Cox, Little, and O'Shea 1998).

Appendix C

Table C1 presents all 384 solutions to the problem of stiffness synthesis of the DP robot presented in the numerical example of Section 6. The highlighted solutions correspond to the initial data used to set up this example.

Acknowledgment

This research was partially supported by the Israeli Ministry of Science under the French–Israel program.

References

- Adams, W., and Loustanaou, Ph. 1994. *An Introduction to Grobner Bases*, Graduate Studies in Mathematics, Vol. 3, American Mathematical Society.
- Becker, T., and Weispfenning, V. 1993. *Gröbner Bases: A Computational Approach to Commutative Algebra*, Springer-Verlag, Berlin.
- Brodsky, V., Glozman, D., and Shoham, M. 1998. Double Circular-Triangular Six-Degrees-of-Freedom Parallel Robot. In J. Lenarcic and M.L. Husty, eds., *ARK—Advances in Robot Kinematics*. Kluwer Academic, Dordrecht, pp. 155–164.
- Buchberger, B. 1965. *An Algorithm for Finding a Basis for Residue Class Ring of a Zero-Dimensional Polynomial Ideals*. Ph.D. thesis, University of Innsbruck, Institute for Mathematics (in German).
- Ciblak, N., and Lipkin, H. 1999. Synthesis of Cartesian stiffness for robotic applications. In *Proceedings of the IEEE International Conference on Robotics and Automation*, Vol. 3, pp. 2147–2152.
- Cox, D., Little, J., and O’Shea, D. 1998. *Using Algebraic Geometry*, Graduate Texts in Mathematics, No. 185, Springer-Verlag, Berlin.
- Daniali, M.H.R., Zsombar-Murray, P.J., and Angeles, J. 1993. The kinematics of a three DoF planar and spherical double triangular parallel manipulators. In J. Angeles, P. Kovacs, and G. Hommel, eds., *Computational Kinematics*, Kluwer Academic, Dordrecht, pp. 153–164.
- Du Plessis, L. J., and Snyman, J. A. 2002. Design and optimum operation of a reconfigurable planar Gough–Stewart machining platform. In H. Neugebauer, ed., *Proceedings of PSK2002: Development Methods and Application Experience of Parallel Kinematics*, pp. 729–749.
- Gosselin, C. 1990. Stiffness mapping for parallel manipulators. *IEEE Transactions on Robotics and Automation* 6(3):377–383.
- Heck, A. 1997. Bird’s-eye view of Grobner bases. *Nuclear Instruments and Methods in Physics Research A* 389:16–21.
- Huang, S., and Schimmels, J. 1998a. The bounds and realization of spatial stiffnesses achieved with simple springs connected in parallel. *IEEE Transactions on Robotics and Automation* 14(3):466–475.
- Huang, S., and Schimmels, J. 1998b. Achieving an arbitrary spatial stiffness with springs connected in parallel. *Journal of Mechanical Design* 120:520–526.
- Kim, W.-K., Lee, J.-Y., and Yi, B.-J. 1997. Analysis for a planar 3 degree-of-freedom parallel mechanism with actively adjustable stiffness characteristics. In *IEEE International Conference on Robotics and Automation*, pp. 2663–2670.
- Kock, S., and Schumacher, W. 1998. A parallel x-y manipulator with actuation redundancy for high-speed and active-stiffness applications. In *IEEE International Conference on Robotics and Automation*, Vol. 2, pp. 2295–2300.
- Loncaric, J. 1985. *Geometrical Analysis of Compliant Mechanisms in Robotics*, Ph.D. Dissertation, Harvard University.
- Mason, M., and Salisbury, K. 1985. *Robot Hands and the Mechanics of Manipulation*, MIT Press, Cambridge, MA.
- Merlet, J.-P. 1989. Singular configurations of parallel manipulators and grassmann geometry. *International Journal of Robotics Research* 8(5):45–56.
- Merlet, J.-P. 2000. *Parallel Robots*, Kluwer Academic, Dordrecht.
- Merlet, J.-P., Preng, M.-W., and Daney, D. 2000. Optimal trajectory planning of a 5-axis machine-tool based on a 6-axis parallel manipulator. In J. Lenarcic and M.M. Stanisic, eds., *Advances in Robot Kinematics*, Kluwer Academic, Dordrecht, pp. 315–322.
- Möller, H. M. 1998. Gröbner bases and numerical analysis. In B. Buchberger and F. Winkler, eds., *Gröbner Bases and Applications*, Lecture Note Series 251, London Mathematical Society, pp. 159–178.
- Möller, H. M., and Stetter, H. J. 1995. Multivariate polynomial equations with multiple zeros solved by matrix eigenproblems. *Numerical Mathematics* 70:311–329.
- Neilsen, J., and Roth, B. 1999. On the kinematic analysis of robotic mechanisms. *International Journal of Robotics Research* 18(12):1147–1160.
- Patterson, T., and Lipkin, H. 1990. A classification of robot compliance. *ASME Journal of Mechanical Design* 115:581–584.
- Patterson, T., and Lipkin, H. 1993. Structure of robot compliance. *ASME Journal of Mechanical Design* 115:576–580.
- Pottman, H., Peternell, M., and Ravani, B. 1999. An introduction to line geometry with applications. *Computer-Aided Design* 31:3–16.
- Raghavan, M., and Roth, B. 1995. Solving polynomial systems for the kinematic analysis and synthesis of mechanisms and robot manipulators. *Transactions of ASME, Special 50th Anniversary Design Issue* 117:71–79.
- Roberts, G. R. 1999. Minimal realization of a spatial stiffness matrix with simple springs connected in parallel. *IEEE Transactions on Robotics and Automation* 15(5):953–958.
- Simaan, N., Glozman, D., and Shoham, M. 1998. Design considerations of new six-degrees-of-freedom parallel robots. In *Proceedings of the IEEE International Conference on Robotics and Automation*, Vol. 2, pp. 1327–1333.
- Simaan, N., and Shoham M. 2002. Stiffness synthesis of a variable geometry planar robot. In J. Lenar and F. Thomas, eds., *Advances in Robot Kinematics: Theory and Applications*, Kluwer Academic, Dordrecht, pp. 463–472.

- Simaan, N., and Shoham M. 2003. Geometric interpretation of the derivatives of parallel robot's Jacobian matrix with application to stiffness control. *ASME Journal of Mechanical Design* 125:33–42.
- Stetter, H. J. 1993. Multivariate polynomial equations as matrix eigenproblems. In *Contributions in Numerical Mathematics*, World Scientific Series in Applicable Analysis (WSSIAA), Vol. 2, pp. 355–371.
- Tsai, L.-W. 1999. *Robot Analysis—The Mechanics of Serial and Parallel Manipulators*, Wiley, New York.
- Wagner, E. R., and Cooney, C. E. 1997. Cardan Hooke universal joint. In *Universal Joint and Driveshaft Design Manual*, Advances in Engineering Series, No 7, SAE publication, pp. 39–43.
- Yi, B., Freeman, R. A., and Tesar, D. 1989. Open-loop stiffness control of overconstrained mechanisms/robotic linkage systems. In *Proceedings of the IEEE International Conference on Robotics and Automation*, pp. 1340–1345.
- Yi, B., and Freeman, R. A. 1992. Synthesis of actively adjustable springs by antagonistic redundant actuation. *ASME Journal of Dynamic Systems, Measurement and Control* 114:454–461.
- Yi, B. J., and Freeman, R. A. 1993. Geometric characteristics of antagonistic stiffness in redundantly actuated mechanisms. In *Proceedings of the IEEE International Conference on Robotics and Automation*, pp. 654–661.
- Zhiming, J., and Song, Ph. 1998. Design of a reconfigurable platform manipulator. *Journal of Robotic Systems* 15(6):341–346.
- Zhiming, J., and Zhenqun, L. 1999. Identification of placement parameters for modular platform manipulators. *Journal of Robotic Systems* 16(4):227–236.